

Multi-channel EEG analyses via dynamic regression models with time-varying lag/lead structure

Raquel Prado^{*†}, Mike West[‡] and Andrew D. Krystal[§]

Summary

Multiple time series of scalp electrical potential activity are generated routinely in electroencephalographic (EEG) studies. Such recordings provide important, non-invasive data informing on brain function in human neuro-psychiatric disorders. Analyses of EEG traces aim to isolate characteristics of their spatio-temporal dynamics that may be useful in diagnosis, may improve the understanding of the underlying neurophysiology, or that may improve treatment through identifying predictors and indicators of clinical outcomes. In this applied context, we discuss the development and application of novel, non-stationary time series models for multiple EEG series generated from individual subjects in a clinical neuropsychiatric setting. The subjects are depressed patients experiencing generalized tonic-clonic seizures elicited by electroconvulsive therapy (ECT) as antidepressant treatment. EEG data routinely recorded during such ECT seizures have previously been explored in a number of studies suggesting that deeper analysis of the spatio-temporal properties of multiple EEG traces have promise for improving our understanding of the remarkable but poorly understood therapeutic effects of ECT. In addition, there is evidence that such analyses may be helpful for improving the effectiveness of the treatment while decreasing side-effects. Two varieties of models – dynamic latent factor models and dynamic regression models – are introduced and studied. We discuss model motivation and form, and aspects of statistical analysis including parameter identifiability, posterior inference and implementation of these models via Markov chain Monte Carlo (MCMC) techniques. In an application to the analysis of a typical set of nineteen EEG series recorded during an ECT seizure at different locations over a patient’s scalp, these models reveal time-varying features across the multiple series that are strongly related to electrode placement around the scalp. In this application we illustrate various model outputs, the exploration of such time-varying spatial structure and its relevance in the ECT study, and discuss the potential uses of such methods as a clinical aid in ECT work and in basic EEG research in general.

Keywords: Bayesian inference; Non-stationary time series; Dynamic linear models; Dynamic latent factors; Electroencephalography; Electroconvulsive therapy; Markov chain Monte Carlo; Time series decomposition.

^{*}*Address for correspondence:* Departamento de Cómputo Científico y Estadística, Universidad Simón Bolívar, Apartado 89000, Caracas, Venezuela. *E-mail:* raquel@cesma.usb.ve.

[†]Centro de Estadística y Software Matemático and Departamento de Cómputo Científico y Estadística, Universidad Simón Bolívar, Venezuela.

[‡]Institute of Statistics and Decision Sciences, Duke University, USA.

[§]Department of Psychiatry and Behavioral Sciences, Duke University Medical Center, USA.

1 Introduction

Multichannel electroencephalographic (EEG) recordings arise from the simultaneous measurement of electrical potential fluctuations at a number of sites on the scalp of a human subject and represent important tools in neuro-psychiatric research. Analysis of such data is presently the least expensive and most widely available way to effectively and non-invasively study human brain function. For a useful, recent collection of articles on analysing EEG data, see Angeleri *et al.* (1997).

One area where the study of brain function through multichannel EEG is particularly promising is in studies of brain seizures induced via electroconvulsive therapy (ECT) as part of the treatment of depression. ECT involves the electrical induction of a series of generalized tonic-clonic seizures for therapeutic purposes and is the most effective known treatment for patients suffering from major depression (Weiner and Krystal 1994). However, the mechanisms of action of this remarkably effective treatment remain poorly understood and there is a need for the development of markers for the prediction and indication of therapeutic response. A number of studies have suggested that the therapeutic effects of ECT seizures may be associated with changes in brain function that are manifest in terms of various EEG features: changes in the patterns of evolution of spectral content over time, changes and differences in raw amplitude of EEG waveforms recorded at different scalp locations, and the relationships between activity among channels (see the review, for example, in Krystal *et al.* 1999). However, prior work has generally focussed on single or double channel EEG recordings, and this limits the capacity to reflect the complex spatio-temporal dynamics of brain activity. In our previous work we have demonstrated the usefulness of various classes of dynamic models for the analysis of univariate EEG studies and begun exploratory studies of the relationships between multiple traces on a single subject (West *et al.* 1999, Prado and West 1997 and Krystal *et al.* 1996). Here we describe further development and application of more formal multivariate dynamic models.

The EEG data studied here is part of a full data set, code named Ictal19, that corresponds to records of 19 EEG channels recorded in 8 subjects in each of 3 different states: while awake, with eyes closed, prior to receiving an electrical stimulus; after methohexital anaesthesia administration but prior to the electrical stimulus; and, finally, during an ECT seizure (Krystal *et al.* 1996, Zoldi *et al.* 1996). During each induced seizure, 19 parallel series were recorded simultaneously from 19 Ag/AgCl electrodes of the International 10-20 EEG System, located around and over the patient's scalp utilising a linked-ear reference and two additional channels dedicated to detecting eye-movement artifacts (Krystal *et al.* 1996). Here we study the 19 EEG traces recorded in one seizure of one of the patients. The purpose of the study is explore commonalities and differences across the 19 traces, and to characterise aspects of the temporal dynamics that aid in understanding the physiology that drives the antidepressant effectiveness of electroconvulsive therapy.

The EEG measurements record fluctuations in levels of cortical electrical activity, as measured at the scalp locations. Typical traces exhibit highly periodic fluctuations with power across a continuum of frequencies and with time-variations in spectral structure. In the neuro-psychiatric communities, EEG activity is loosely categorised into four main frequency ranges: the low frequency *delta* band, of roughly 0-4Hz; the *theta* band, of roughly 4-8Hz; the *alpha* band, of roughly 8-13Hz, and the *beta* band, of more than 13Hz. Often the appearance

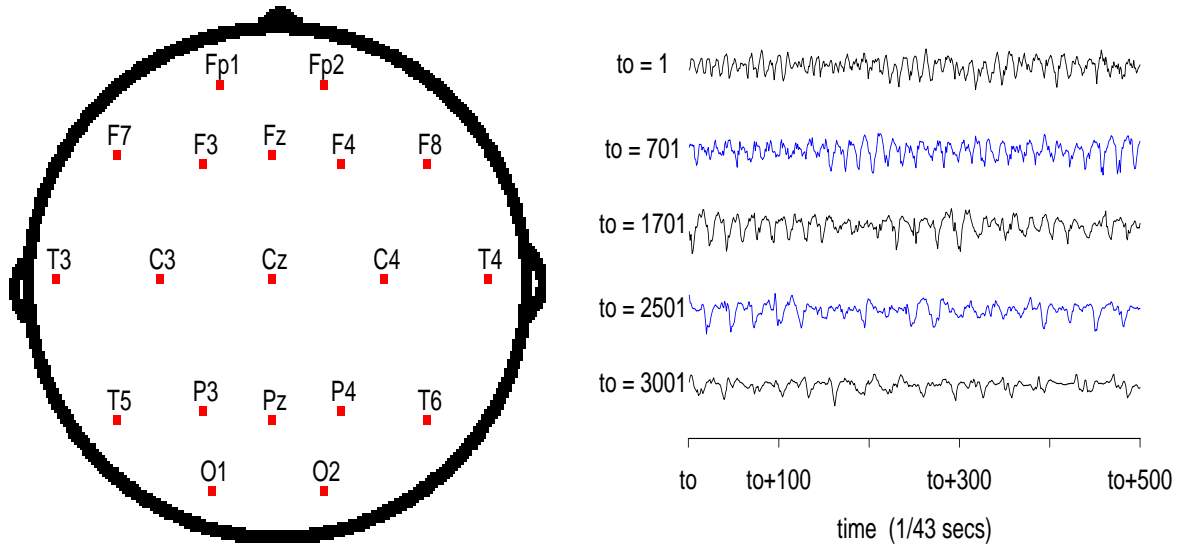


Figure 1: *Left frame*: schematic representation of the Ictal19 electrode placement. *Right frame*: sections of EEG voltage levels recorded during an ECT seizure at site \mathbf{F}_7

of activity in a specific band characterises a particular physiological state (Dyro 1989).

The left frame in Figure 1 shows a schematic representation of the approximate locations of the 19 electrodes over the scalp. By convention, electrodes located on the left side are odd numbered while those on the right side are even numbered. The capital letters \mathbf{F} , \mathbf{Fp} , \mathbf{P} , \mathbf{T} , \mathbf{C} and \mathbf{O} refer to the *frontal*, *prefrontal*, *parietal*, *temporal*, *central* and *occipital* cortical regions (Dyro 1989). Electrodes down the centre of the scalp are labelled with the letter \mathbf{z} , in particular, channel \mathbf{C}_z is referred to as the vertex in EEG nomenclature. Prior to recording, EEG signals are amplified and filtered with a bandpass of 1.6-70Hz, are then stored on magnetic tape and digitised off-line at 256Hz with 12bit accuracy. Manual artifact rejection was performed (by A.D.K.) prior to analysing the data in order to remove artifacts present in the signals due to patient movement and other laboratory interference.

ECT seizure EEG records usually last between 0.5 and 3 minutes therefore a typical series constitutes between 15,000 and 50,000 observations. We study sub-sampled series with between 40 to 50 equally spaced observations per second. After sub-sampling we deal with series of a few thousand observations that produce graphical displays that are essentially indistinguishable from the graphs produced by the original data. The right frame in Figure 1 shows sections of an EEG recorded at site \mathbf{F}_7 . The original recordings of about 26,000 observations were sub-sampled every sixth observation from the highest amplitude portion of the seizure resulting in a series of 3,600 observations. The graph shows sections of 500 consecutive observations taken from near the start, two central sections and close to the end of the seizure period. The EEG series displays typical high frequency oscillations at the beginning that slowly decay into lower frequencies accompanied by an increase in the amplitude of the signal relative to the amplitude observed at initial states, until it finally

decreases towards the end of the seizure. These general features are consistent across the 19 traces from this subject/seizure, suggesting the existence of a common underlying process driving the behaviour of the multiple series. However, variations over time in the frequency content and amplitude fluctuations appear to differ markedly across channels.

Section 2 summarises previous analyses of some of the Ictal19 data based on univariate time-varying autoregressive (TVAR) models and decompositions (Prado and West 1997, West *et al.* 1999). The use of TVAR decompositions in isolating common features across multiple EEG series is highlighted. In Section 3, we begin by exploring latent factor models as a multivariate modelling approach to recover and describe latent processes underlying multiple series. We then discuss dynamic regression models with time-varying lags/leads that describe additional structure linking the series that TVAR and factor models are unable to capture. Finally, Section 4 provides conclusions, comments and some discussion of future directions.

2 Univariate TVAR models and decompositions

Previous studies of EEG series using TVAR models have been most encouraging in delivering useful insights into EEG structure and their connections with ECT outcomes. Sections of some of the series from the Ictal19 data set have been analysed using this approach in Prado and West (1997), West *et al.* (1999) and Krystal *et al.* (1999). A key aspect of those analyses is the use of time series decomposition methodology to explore non-stationary time:frequency structure of latent components of the EEG traces. In this aspect, the work extends the uses of TVAR models that have been earlier used and validated as empirical representations of other kinds of EEG data (Gersch 1985, Gersch 1987, Kitagawa and Gersch 1996).

In Prado and West (1997) selected portions of Ictal19 series are analysed using univariate TVAR models in which the AR parameter vector evolves stochastically in time as a random walk. Formally, write x_t for observed value of an EEG series at time t , on an equally-spaced time scale $t = 0, 1, \dots$. The TVAR(p) model is $x_t = \mathbf{x}_t' \boldsymbol{\phi}_t + \nu_t$ and $\boldsymbol{\phi}_t = \boldsymbol{\phi}_{t-1} + \boldsymbol{\omega}_t$ where $\mathbf{x}_t = (x_{t-1}, \dots, x_{t-p})'$, $\boldsymbol{\phi}_t$ is the “instantaneous” AR parameter vector at time t , $\{\nu_t\}$ is a sequence of independent normal *observation innovations* with possibly time-varying variances σ_t^2 , and $\{\boldsymbol{\omega}_t\}$ is a sequence of independent p -vector *parameter innovations*. The degree to which $\boldsymbol{\phi}_t$ and σ_t^2 vary is determined via standard discount methods (West and Harrison 1997). Suitable values of discount factors and model order p may be assessed via marginal likelihoods as discussed in West *et al.* (1999). Once the EEG series are modelled via TVAR models the focus is on exploring time:frequency structure of latent processes using decompositions based on the eigenstructure of the TVAR evolution matrices of the dynamic model. The basic result for TVAR models states that (West *et al.* 1999)

$$x_t = \sum_{j=1}^{p_z} z_{t,j} + \sum_{j=1}^{p_y} y_{t,j}$$

where p_z is the number of pairs of complex characteristic roots of the instantaneous AR characteristic polynomial defined by $\boldsymbol{\phi}_t$ at time t , and p_y is the number of real characteristic roots, such that $2p_z + p_y = p$. In general the processes $z_{t,j}$ and $y_{t,j}$ are, under certain conditions discussed in West *et al.* (1999), dominated by TVARMA(2,1) and TVAR(1) processes,

respectively. The autoregressive structure of each $z_{t,j}$ process is quasi-periodic, with time-varying characteristic frequency and modulus $\omega_{t,j}$ and $r_{t,j}$. Figure 2 displays the estimated decomposition and trajectories of the frequency and modulus of the lowest frequency component in the analysis of series \mathbf{C}_3 based on a TVAR(12) model. The top frame graphs, from the bottom up, the data, followed by the estimated $z_{t,j}$ in order of increasing characteristic frequency. Component (1) corresponds to the delta/slow-wave whose instantaneous characteristic frequency and modulus are displayed in the bottom frames. This component lies in the *delta* range which is characteristic of slow-waves manifest, in particular, in the middle and late phases of effective ECT seizures (Niedermeyer 1993; Staton *et al.* 1981; Weiner *et al.* 1991; Weiner and Krystal 1993). Component (1) dominates in amplitude and has moduli values higher than 0.9 during most of the seizure course (see Figure 2). Component (2) lies in the *theta* band and is much lower in amplitude and modulus than component (1). Higher frequency components also appear in the decomposition and have much lower amplitudes than the lower frequency components that really characterise the seizure episode.

Repeating the TVAR(12) analysis and exploring the decompositions for the 19 EEG series we find similarities in patterns of behaviour of the dominant frequency components across channels (see Prado and West 1997). As we move through the time course of the seizure, the instantaneous AR characteristic polynomials exhibit and maintain at least two dominant pairs of complex conjugate roots across the 19 series – dominant in the sense of having higher moduli and lower frequencies than the remaining roots. These two pairs of characteristic roots correspond to the dominant “seizure” latent processes living in the *delta* and *theta* frequency bands. The ranges of the corresponding frequencies are consistent across the 19 channels, varying over time between one and five cycles according to the gradual decay as the seizure dies off – see Figure 2. The moduli trajectories of the lowest frequency components are also similar across the 19 channels. These common patterns exhibited by the dominant components in the decompositions suggest the notion of the existence of at least one latent quasi-periodic process underlying the 19 series. Modelling the traces via *latent factor models*, with one or two common latent processes or “factors” driving the series, therefore seems appropriate. This direction was anticipated in Prado and West (1997), and is now explored in the development of dynamic factor models and dynamic regressions with time-varying lag/lead structures.

3 Multivariate dynamic structure

3.1 Factor models and autoregressions

A relatively simple model, based on the results obtained via univariate TVAR analyses of the Ictal19 data, is suggested as a first step towards a characterisation of the system underlying the 19 series. In more generality, suppose we have m series under study, and let $y_{i,t}$ be the observation recorded at time t on electrode/channel i , ($i = 1, \dots, m$). Assume that the system under study is characterised by a latent process x_t such that, for each $i = 1, \dots, m$,

$$\begin{aligned} y_{i,t} &= \beta_i x_t + \nu_{i,t} \\ x_t &= \sum_{j=1}^p \phi_{t,j} x_{t-j} + \eta_t \\ \phi_t &= \phi_{t-1} + \omega_t \end{aligned} \tag{1}$$

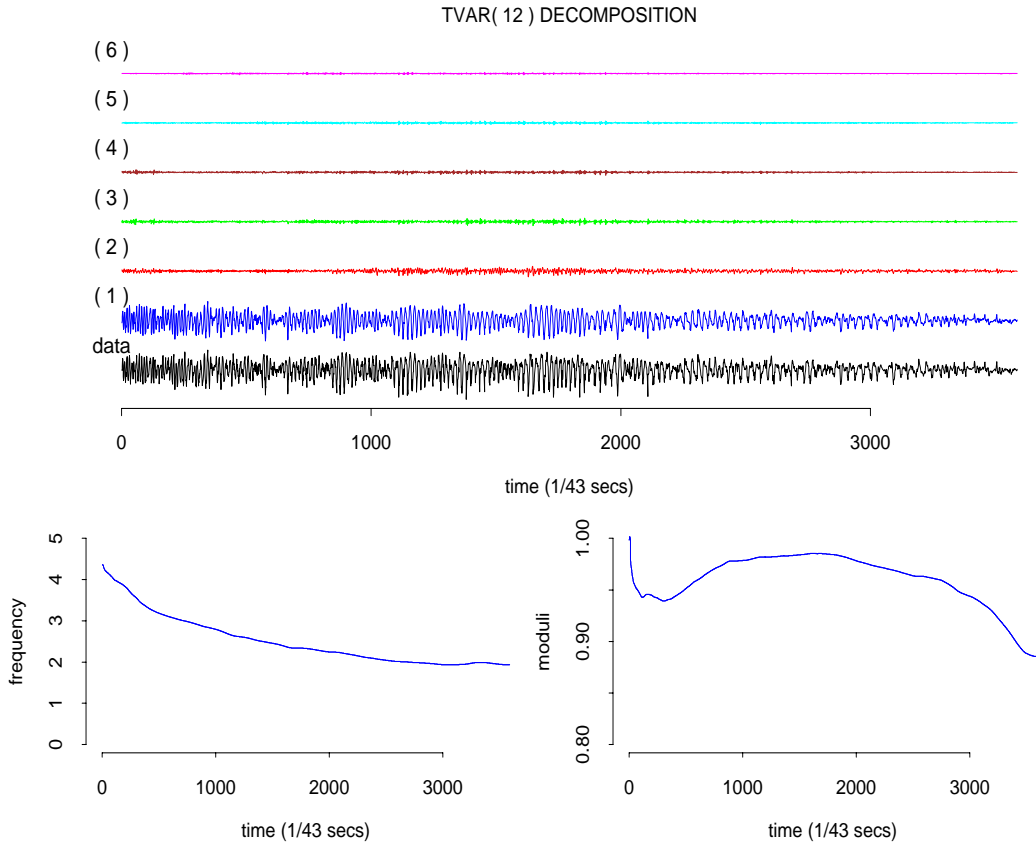


Figure 2: *Top frame*: data and estimated components in the decomposition of EEG series \mathbf{C}_3 based on a TVAR(12) model. From the bottom up, the graph displays the time series followed by the six estimated components in order of increasing characteristic frequency. Component (1) lies in the *delta* (0-4Hz) band for most of the seizure course. Components (2) and (3) lie in the *theta* (4-8Hz) band while component (4) lies in the *alpha* (8-13Hz) band. Components (5) and (6) belong to the *beta* (higher than 13Hz) frequency band. *Bottom frames*: Trajectories of the estimated characteristic frequency and modulus of the lowest frequency component in series \mathbf{C}_3 .

where the β_i 's are regression parameters or factor weights. The unobservable process x_t has a TVAR(p) structure modelling the common ‘‘seizure’’ waveforms that consistently appeared in the decompositions of the 19 EEG series. The TVAR parameter vector $\boldsymbol{\phi}_t = (\phi_{t,1}, \dots, \phi_{t,p})'$ follows a random walk and $\nu_{i,t}$, η_t and $\boldsymbol{\omega}_t$ are independent and mutually independent, zero-mean Gaussian innovations; we write these distributions as $N(\nu_{i,t}|0, v_i)$, $N(\eta_t|0, s)$ and $N(\boldsymbol{\omega}_t|0, \mathbf{U}_t)$ for some observational variances v_i , TVAR innovation variance s and system variance-covariance matrices \mathbf{U}_t controlling the variability of $\boldsymbol{\phi}_t$. Note that s is constant in our analyses here, though could more generally be time-varying.

Model (1) is a dynamic factor model with a single factor process x_t and constant factor weights, and relates to various previous approaches to latent factor modelling. Most prior work has focused on stationary processes, however, rather than the non-stationary, time-varying parameter versions here. Important contributions are those of Peña and Box (1987) and Tiao and Tsay (1989), for example. Extensions to include $k > 1$ latent factors, possibly time-varying factor weights and connections between factor models and TVARMA models are mentioned in Prado and West (1997). Following the notation in Prado and West (1997), a rather general dynamic factor model with $k > 1$ factors and m observed series can be written in matrix form

$$\mathbf{y}_t = \mathbf{B}_t \mathbf{x}_t + \boldsymbol{\nu}_t, \quad (2)$$

where $\mathbf{y}_t = (y_{1,t}, \dots, y_{m,t})'$ is the m -dimensional vector of observations at time t , $\mathbf{B}_t = [\boldsymbol{\beta}_{1,t}, \dots, \boldsymbol{\beta}_{k,t}]$ is an $m \times k$ matrix with $\boldsymbol{\beta}_{j,t} = (\beta_{1,j,t}, \dots, \beta_{m,j,t})'$ and $\beta_{i,j,t}$, the factor weight relating the i -th observation $y_{i,t}$ to the j -th factor $x_{j,t}$ at time t . It is usually assumed that $\mathbf{V}_t = \text{diag}[v_{1,t}, \dots, v_{m,t}]$ so that the dependencies among the $y_{i,t}$'s are due exclusively to the $x_{j,t}$'s. Additionally, $\mathbf{x}_t = (x_{1,t}, \dots, x_{k,t})'$ can be modelled via general dynamic linear models (West and Harrison 1997). Modelling each $x_{j,t}$ as a TVAR seems reasonable in the EEG framework. One important class of factor models is that based on lagged latent factors. Suppose for instance that $x_{1,t} = x_t$ and $x_{2,t} = x_{t-1}, \dots, x_{k,t} = x_{t-k+1}$. Then, if x_t is a TVAR process, it follows that $y_{i,t}$ is a TVARMA(p, q) with $q = \max(p, k)$. It is typically assumed that $k \ll m$. In the EEG context one or two latent factors may be enough to explain the underlying structure driving the behaviour of the multiple signals and $k > 2$ but surely $k < 19$ factors may be needed to account for lagged values of the latent processes.

We begin by exploring the simplest factor model described in (1) taking $v_i = v$ and $s_t = s$ for all i and t . Note that model (1) is not identified. In fact, if we consider $\beta_i^* = \beta_i/c$ for some $c \neq 0$ the model can be written in terms of β_i^* , $x_t^* = cx_t$ and $\eta_t^* = c\eta_t$. To resolve this parameter identification issue we impose restrictions on the factor weights via $\beta_i = 1$ for a specific channel i . In addition, we assume that the signal-to-noise ratio $r = s/v$ is a fixed known quantity. With this model specification, we can proceed to posterior analysis and inference once priors for model parameters are specified. In our analyses we routinely use standard reference priors for the β_i and v , and relatively diffuse normal priors for $\boldsymbol{\phi}_0$. Posterior simulation methods based on basic DLM theory (West and Harrison 1997) and standard Gibbs sampling techniques for state space models (Carter and Kohn, 1994; Frühwirth-Schnatter, 1994) are used to obtain samples from the posterior distributions, and so lead to summaries for parameters estimation. Further details of the conditional posteriors required for this MCMC simulation analysis appear in the Appendix.

Models with a single latent factor, identifying constraint $\beta_{\mathbf{Cz}} = 1$, and different fixed

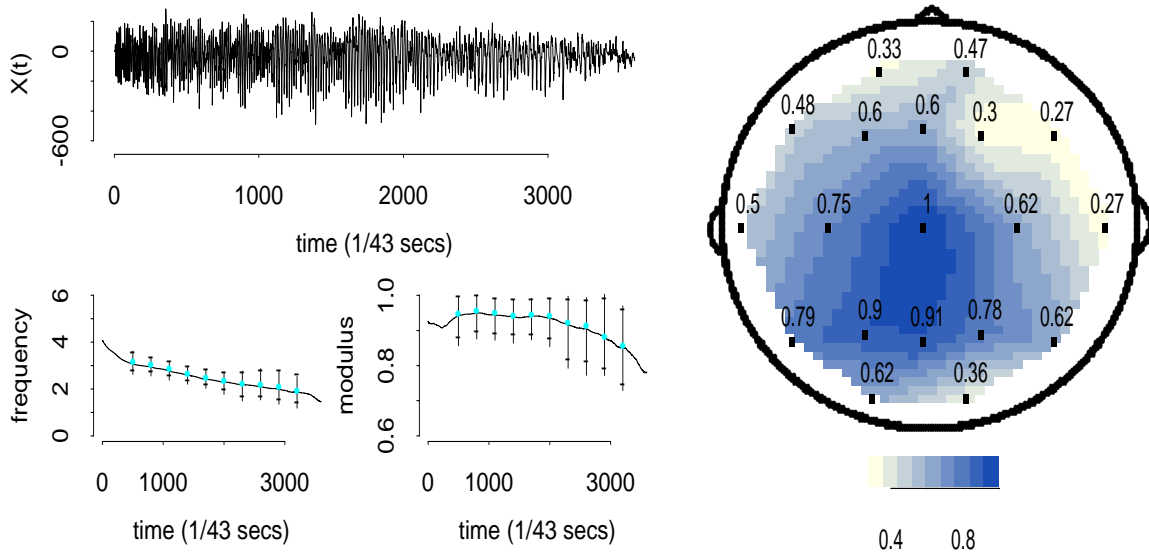


Figure 3: *Left frame*: Estimated latent factor process (top); Frequency trajectory of the estimated dominant component for the latent process and approximate 95% posterior intervals at selected points (down left); Modulus trajectory of the estimated dominant component for the latent process and approximate 95% posterior intervals at selected points (down right). *Right frame*: estimated posterior means of the factor weights for the 19 EEG channels.

model order values $p \in \{4, 5, 6, 7, 8\}$ were fitted to the 19 EEG series. There is a recent and growing literature on incorporating model order uncertainty for standard AR models via MCMC methods using ideas of stochastic variable selection and reversible jump (see for instance Huerta and West 1999 and Troughton and Godsill 1997). However, these approaches do not deal with model order uncertainty in TVAR models. Extensions to factor models that take into account model order uncertainty in the TVAR latent structure are certainly imaginable, but will lead to very significant increases in complexity and computational demands of the posterior simulation algorithms. It is very questionable whether such costs are at all worthwhile, and we currently are more than satisfied with exploring a range of models with different orders in order to understand how resulting inferences depend on the choice and over what data-supported ranges they are insensitive. A single discount factor approach (West and Harrison 1997) was used to specify the evolution variance matrix sequence $\{\mathbf{U}_t\}$. Various choices of the implied discount factor δ , and r were explored by allowing these parameters to take values in intervals chosen based on the univariate TVAR analyses summarised in Section 2. Appropriate values are explored by evaluating the corresponding joint marginal likelihood functions from the univariate analyses. From such analyses we inferred that appropriate values of δ lie in the 0.994-0.996 range, while appropriate values of r lie on the 5-15 range. Parameters in these ranges produced estimates of x_t whose amplitudes are similar to the amplitudes of the processes obtained by adding the first four dominant components in the univariate TVAR decompositions of the 19 EEG series.

Figure 3 displays graphs summarising the results obtained from a single latent factor

model with $p = 6$, $\delta = 0.994$ and $r = 10$. The convergence tests and results are based on a posterior sample of 500 draws taken from 3,000 iterations of the Gibbs sampler after a burn-in of 3,000 iterations. In order to explore the convergence of the chain various diagnostics, in addition to autocorrelation and trace plots for some of the model parameters, were carried out. In particular, the Geweke convergence diagnostic, the Heidelberger and Welch stationary test and the Raftery and Lewis diagnostic (see Brooks and Roberts 1999), were performed for sequences corresponding to model parameters $\phi_{1010,1}$, $\beta_{\mathbf{P}_3}$, x_{701} and x_{1231} . This was done using Bayesian Output Analysis (BOA) Program version 0.4.3 for R (<http://www.public-health.uiowa.edu/boa>). The 500 draws for the posterior sample were taken every sixth iteration of the 3,000 obtained from the Gibbs sampler after the burn-in period. All the MCMC sequences considered passed the Heidelberger and Welch convergence test and neither the Geweke nor the Raftery and Lewis diagnostics gave evidence that convergence was not achieved for such sequences.

The graph at the top left frame in Figure 3 displays the time trajectory of the estimated posterior mean of x_t , \hat{x}_t . The TVAR(6) structure assumed for x_t exhibits two pairs of complex characteristic roots across the time period of the data. Time trajectories of the frequency and modulus of the lowest frequency component of \hat{x}_t are shown down in the left frame of Figure 3. This component exhibits the same general features displayed by the slow/wave dominant components that appeared in the univariate TVAR decompositions of the 19 EEG series. The frequency decreases over time and lies in the *delta* range (0-4Hz) during the seizure course, while the instantaneous characteristic modulus consistently takes values above 0.85. The vertical bars represent approximate 95% posterior intervals for the instantaneous frequency and modulus at the selected time points, so providing pointwise indications of uncertainties about the estimated trajectories. The right frame in Figure 3 shows the estimated posterior means of the factor weights β_i for $i = 1, \dots, 19$, denoted by $\hat{\beta}_i$. Note that we set $\beta_{\mathbf{C}_z} = 1$. The values displayed at the approximate electrode locations correspond to the $\hat{\beta}_i$. In addition, an image created by linearly interpolating the $\hat{\beta}_i$ over the grid defined by the approximate electrode locations is displayed. This image is simply used to highlight the relationships between the estimated factor weights and is not the result of building into the model a spatial dependence structure on the β_i . Dark intensities correspond to high values of $\hat{\beta}_i$ while light intensities correspond to low values. The graph exhibits a marked pattern of relationship across “neighbouring” channels: channels located closer to \mathbf{C}_z have factor weights closer to the unity. There is also an element of asymmetry evident from this picture. Channels located at right fronto-temporal sites have smaller weights than channels located at left fronto-temporal sites. Approximate 95% posterior intervals were computed for each β_i . The upper bounds of such intervals were lower than the unity in magnitude for all sites. Posterior estimates were calculated for models with $p = 4, \dots, 8$ and different values of r , leading to similar conclusions in terms of the latent quasi-periodic structures of x_t and the relation between the factor weights for the 19 EEG series and the electrode locations.

This analysis with a single factor model reveals relationships between channels – in terms of $\hat{\beta}_i$ – that univariate analyses via TVAR models are not able to capture. However, estimates of the residuals computed for these models exhibit substantial remaining structure. For most of the channels there are quasi-periodic patterns left unexplained by single factor models with constant factor weights. Such patterns in the residuals may be explained in several ways. First, the assumption that one latent factor is enough to explain the structure underlying the

multiple EEG signals is quite simplistic although somehow imperative from the computational viewpoint. Fitting models with more factors is complicated as both parameter identification and interpretability, and computational difficulties increase significantly with the number of factors. A second likely reason for residual correlation structures is the need to allow for factor weights to vary over time. For instance, the ratio between the amplitude of a signal recorded at a given channel and the amplitude of the signal recorded at \mathbf{C}_z does not seem to remain constant over time – on a purely exploratory basis. Additionally, cross-correlograms of the residuals display phase delays between some of the channels that vary throughout the seizure course. In particular, cross-correlograms of the residuals for channels \mathbf{C}_z and \mathbf{Fp}_2 show that the signal recorded at site \mathbf{C}_z seems to be delayed with respect to the signal recorded at site \mathbf{Fp}_2 at central portions of the seizure course, whereas no delays are evident at very early and late portions. Cross-correlograms for channels \mathbf{C}_z and \mathbf{O}_1 show that the signal recorded at \mathbf{O}_1 is delayed with respect to the signal recorded at \mathbf{C}_z for central portions of the seizure, while again there are practically no delays at the beginning and the end of the seizure. This suggests exploring models that explicitly involve time-varying descriptions of the amplitude ratios and lag/lead structures across the channels.

3.2 Dynamic regression models with time-varying lag/lead structures

Consider the model

$$\begin{aligned} y_{i,t} &= \beta_{(i,t)} x_{t-l_{i,t}} + \nu_{i,t} \\ \beta_{(i,t)} &= \beta_{(i,t-1)} + \omega_{i,t} \end{aligned} \quad (3)$$

with $y_{i,t}$ the observation recorded at time t on channel i , and with the following specifications.

- x_t is an underlying process assumed known at each t . This could, for example, be the EEG signal recorded at a particular location on the scalp, or the sum of the first two or three dominant components estimated from the TVAR decomposition of such a signal.
- $l_{i,t}$ is the lag/lead that $y_{i,t}$ exhibits with respect to x_t instantaneously at time t . These parameters are explicitly allowed to be time-varying, and lie in a prescribed set of possible values $l_{i,t} \in \{-k_0, \dots, 0, \dots, k_1\}$. Here $-k_0$ and k_1 are bounds chosen a priori to specify maximum lag/lead values. Changes in lag/lead structure are described via a one-step Markov chain model with specified transition probabilities $p(l_{i,t} = k | l_{i,t-1} = m)$, with $k, m \in \{-k_0, \dots, 0, \dots, k_1\}$.
- $\beta_{(i,t)}$ is the dynamic regression coefficient of x_t for channel i . In particular, if $x_t = y_{i_0,t}$ and $\beta_{(i_0,t)} = 1$ for some channel i_0 and all t , then $\beta_{(i,t)}$ for $i \neq i_0$ is a direct measure of dependence between channels i_0 and i . A random walk is adopted to model the evolution of $\beta_{(i,t)}$, providing adaptation to possible changes of these parameters over time without anticipating specific directions of changes (West and Harrison 1997).
- $\nu_{i,t}$ are i.i.d. zero mean observational error terms with variances v_i and $\omega_{i,t}$ are i.i.d. zero mean system innovations assumed normally distributed with variances $s_{i,t}$.

Given that x_t is assumed known for all t and that $\nu_{i,t}$ and $\omega_{i,t}$ are independent across channels, the equations in (3) describe a collection of univariate models rather than a multivariate

m -dimensional model. Eliminating the lag/lead parameters from the first equation in (3) by taking conditional expectations (with all other parameters fixed) we obtain $E(y_{i,t}|x_{\cdot}, \beta_{\cdot})$ as a weighted average of the lagged and lead values $x_{t+k_0}, x_{t+k_0-1}, \dots, x_t, \dots, x_{t-k_1}$ with weights $p(l_{i,t} = -k_0)\beta_{(i,t)}, \dots, p(l_{i,t} = k_1)\beta_{(i,t)}$. Thus each channel is modelled as a time-varying dynamic regression on past, current and future values of the x_t process, with coefficients reflecting an overall, time-varying level of response $\beta_{(i,t)}$ together with changes in the relevance of lagged and lead values via the $p(l_{i,t} = \cdot)$ terms. Given that x_t is the same fixed underlying process for all channels it is possible to make comparisons of any two channels via $\beta_{(i,t)}$ and $l_{i,t}$, and their estimated trajectories over time. Further model components we need to specify are priors on $\beta_{(i,0)}$, on v_i and the transition probabilities $p(l_{i,t} = k | l_{i,t-1} = m)$. The specification of conditional evolution variances $s_{i,t}$ is handled, as usual, via discount factors. Posterior inferences may be obtained via MCMC algorithms, as detailed in the Appendix.

3.3 The Ictal19 data revisited

Dynamic regression models assuming that x_t is the actual signal recorded at the vertex channel, that is $x_t = y_{t, \mathbf{C}_z}$, were fitted to the Ictal19 data. Relative diffuse normal/inverse-gamma priors were placed on the regression coefficients; normal priors conditional on v_i with means $m_i = 1$ for all i were used to model the regression coefficients. The transition probabilities $p(l_{i,t} | l_{i,t-1})$ were fixed for all t and uniform initial priors $p(l_{i,0} = k | D_0) = 1/(k_1 + k_0 + 1)$ were considered. Discount factors in the range 0.99-0.999, were considered to control the variability of $\beta_{(i,t)}$ over time. Such values were chosen based on exploration of marginal likelihood functions from univariate analyses of models that regress each recorded signal on the signal recorded at \mathbf{C}_z and fixed lagged/leaded values of such signal. Posterior summaries were computed for models with $l_{i,t} \in \{-3, \dots, 3\}$ and transition probabilities such that $p(l_{i,t} = k | l_{i,t-1} = k) \geq 0.999$ and where only movements of the type ‘‘one-step a time’’ are permitted, i.e. $p(l_{i,t} = j | l_{i,t-1} = i) = 0$ for all j such that $j \geq i + 2$ or $j \leq i - 2$. The choice of the set of values that the lags/leads can take is based on previous analyses of the cross-correlogram functions between each channel and \mathbf{C}_z .

The summary graphs displayed in Figures 4, 5 and 6 are based on an analysis with such assumptions. The MCMC analysis produced 3,000 draws from the posterior distributions for each channel taken after a burn-in period of 4,000 iterations. In order to explore MCMC convergence, the Geweke convergence diagnostic, the Heidelberger and Welch stationary test and the Raftery and Lewis diagnostic (see Brooks and Roberts 1999), were performed for some model parameters: v_i for all i , $\beta_{\mathbf{O}_1, 1756}$, $\beta_{\mathbf{O}_1, 3157}$ and $l_{\mathbf{O}_2, 877}$. Again, the BOA Program version 0.4.3 for R was used. Autocorrelations at lags 1, 5, 10 and 50 for each of the sequences of the parameters were very low – always less than 0.07 in absolute value – and similar results were obtained for the cross-correlation of the parameters. All the sequences considered passed the Heidelberger and Welch convergence test and neither the Geweke nor the Raftery and Lewis diagnostics gave evidence that convergence was not achieved for such sequences.

The transition probabilities for the model are displayed in Table 1 and the system discount factors were set to $\delta_i = 0.996$. These transition probabilities impose desirable smoothness restrictions on the evolution of lags/leads but other structures may be considered. The prior distribution is uniform on k for all i , i.e. $p(l_{i,0} = k | D_0) = 1/7$ for all $k \in \{-3, \dots, 3\}$. Figure 4 provides the estimated posterior means of the β_{\cdot} coefficients for the 19 channels at selected

		t				
		$k = -2$	$k = -1$	$k = 0$	$k = 1$	$k = 2$
$t - 1$	$m = -2$	0.9999	0.0001	0.0	0.0	0.0
	$m = -1$	0.00005	0.9999	0.00005	0.0	0.0
	$m = 0$	0.0	0.00005	0.9999	0.00005	0.0
	$m = 1$	0.0	0.0	0.00005	0.9999	0.00005
	$m = 2$	0.0	0.0	0.0	0.0001	0.9999

Table 1: Transition probabilities $p(l_{i,t} = k \mid l_{i,t-1} = m)$.

time points during the seizure. The values displayed at the approximate electrode locations correspond to $\hat{\beta}_{(i,t)}$. Additionally, an image plot created by linearly interpolating the $\hat{\beta}_{(i,t)}$ onto a grid defined by the approximate electrode locations is displayed. Dark intensities match higher coefficient values while light intensities correspond to lower values. Aspects of the temporal:spatio relations between channels are evident from these graphs. In general, a given channel shares more similarities with channels located closer to it. This is consistent with the behaviour observed in the estimated factor weights obtained from the single factor model analyses (see Figure 3). Note also the asymmetry, more evident towards the end of the seizure course, between the estimated coefficients of channels located at the frontal right sites and at the frontal left sites. The values of the coefficients are much smaller for channels **F₄** and **F₈** (right side) than for channels **F₃** and **F₇** (left side).

Figure 5 provides a display of the estimated lags/leads based on posterior means of the l quantities at different time points. If a site displays the lightest intensity at a given t , then the signal recorded at this site is delayed with respect to the signal recorded at **C_z** in two units of time. Signals recorded at occipital sites are delayed in two units of time with respect to the signal recorded at **C_z** at $t = 1000, 1100$ and 1200 . Similarly, if a site shows the darkest intensity at a given t the signal recorded at this site leads the signal recorded at **C_z** in two units of time. Central portions of the seizure display intense lag/lead activity characterised by lags in the occipital regions and leads in the frontal and pre-frontal regions. Again, an image plot is superimposed to provide visual interpolation, although there is no underlying spatial model.

The related Figure 6 displays estimated posterior probabilities on values of the lags and leads over time for channel **O₁** (left frames) and **F_{p2}** (right frames). Channel **O₁** displays the highest estimated posterior probabilities at $k = -2, -1, 0$ while channel **F_{p2}** exhibits the highest probabilities at $k = 0$ for most of the seizure course and at $k = 1$ during brief periods.

In addition, Figure 7 illustrates how the model captures the lag/lead time-varying structure present in the series. The figure displays the EEG traces for channels **O₁** (frames (a) and (b) solid lines) and **C_z** (frames (c) and (d) solid lines) together with the estimated traces for channel **O₁** (dotted lines) during early-middle and middle seizure periods. Clearly, channel **O₁** is delayed with respect to channel **C_z** during some seizure portions and the delay is bigger during early-middle portions (compare frames (c) and (d)). Samples of the standardized residuals were computed from the MCMC sequences and explored using standard residual diagnostics, graphics and correlation analyses. The sampled residuals generally exhibit no obvious residual structure, and cross-correlograms of the residuals displayed no apparent phase delays. However, for some of the channels, in particular for channels **F_{p1}** and **F_{p2}** the

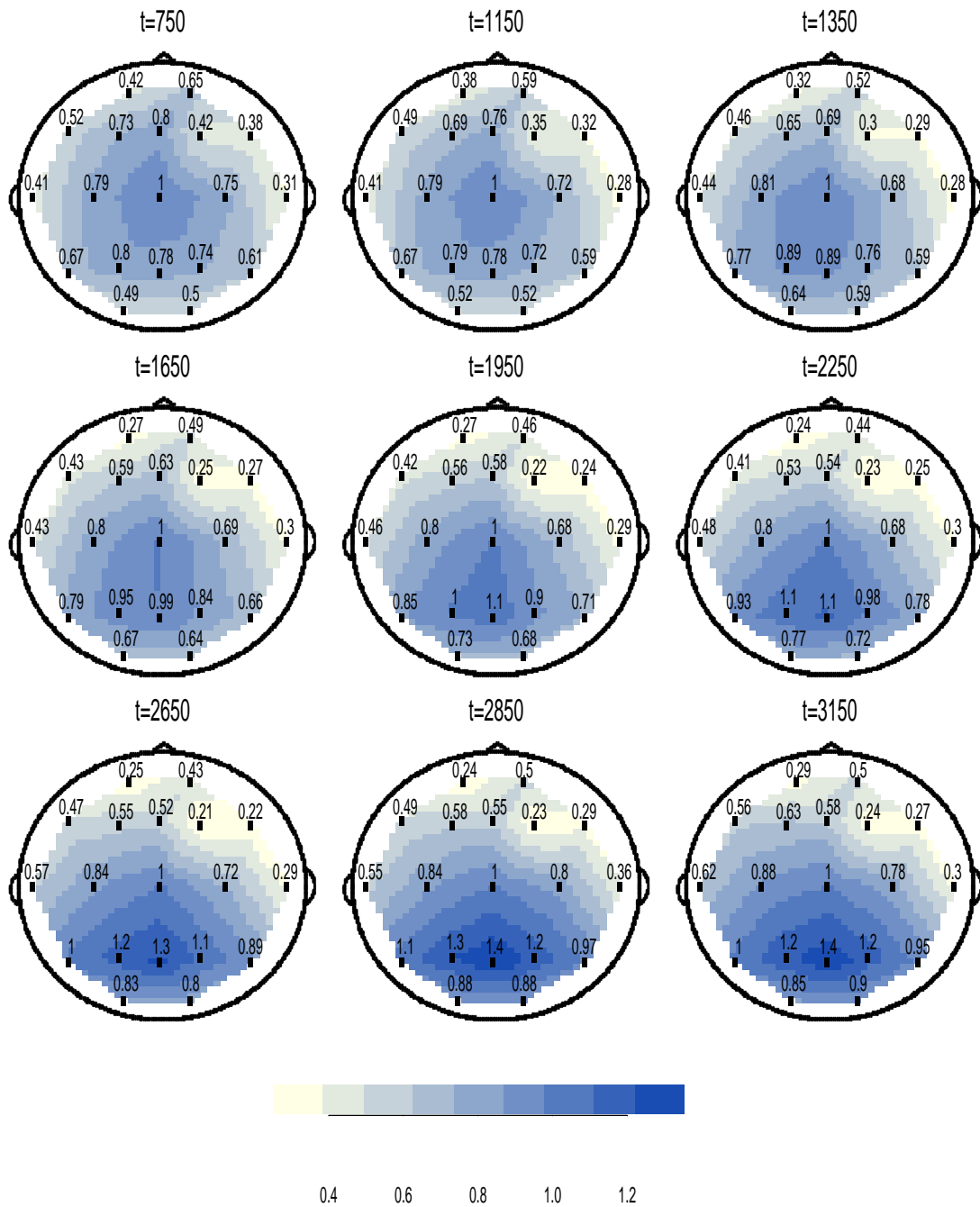


Figure 4: Estimated posterior means of the dynamic factor weights for all channels at selected points during the seizure course.

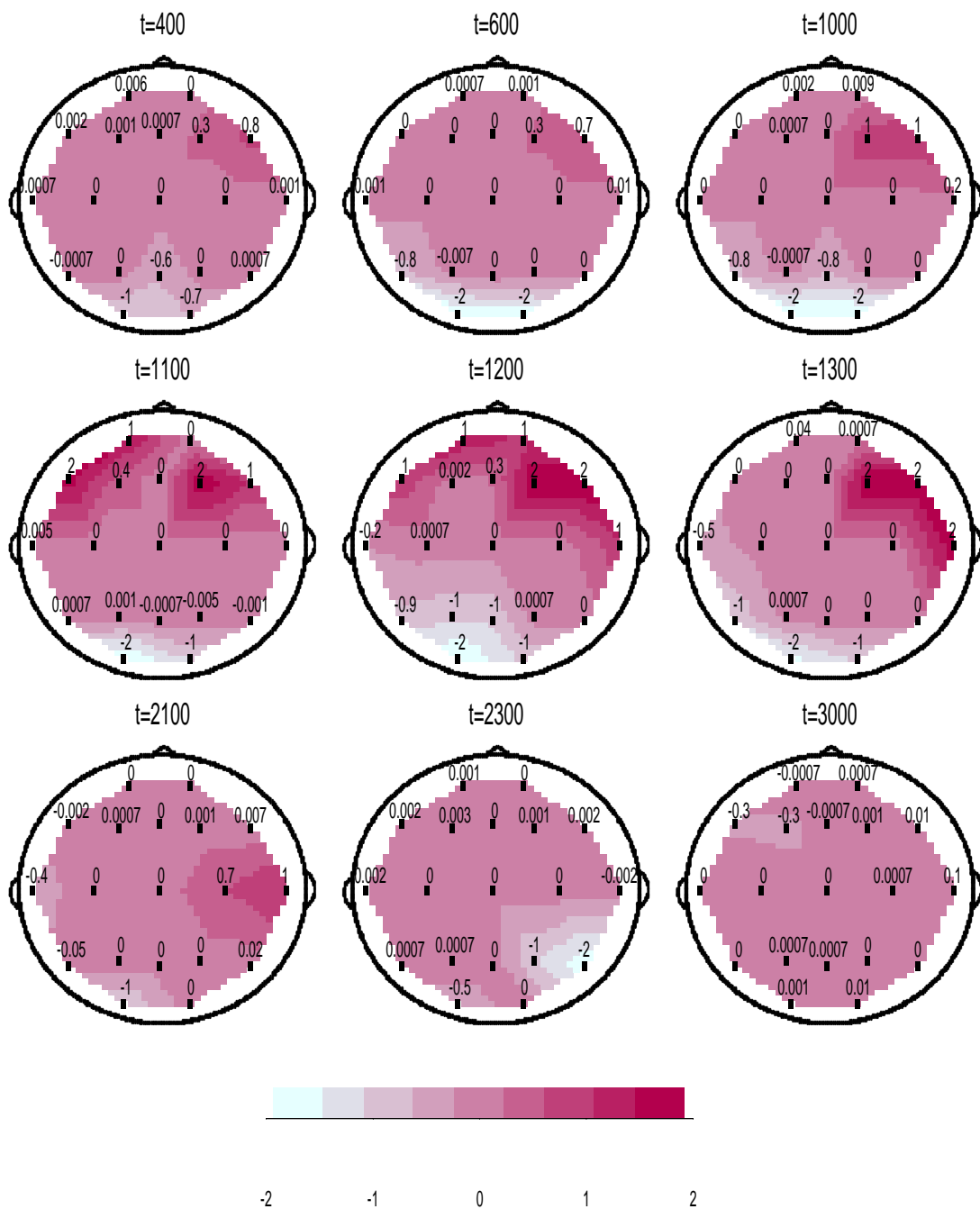


Figure 5: Dynamic lags/leads on the Ictal-19 data set, based on posterior mean estimates.

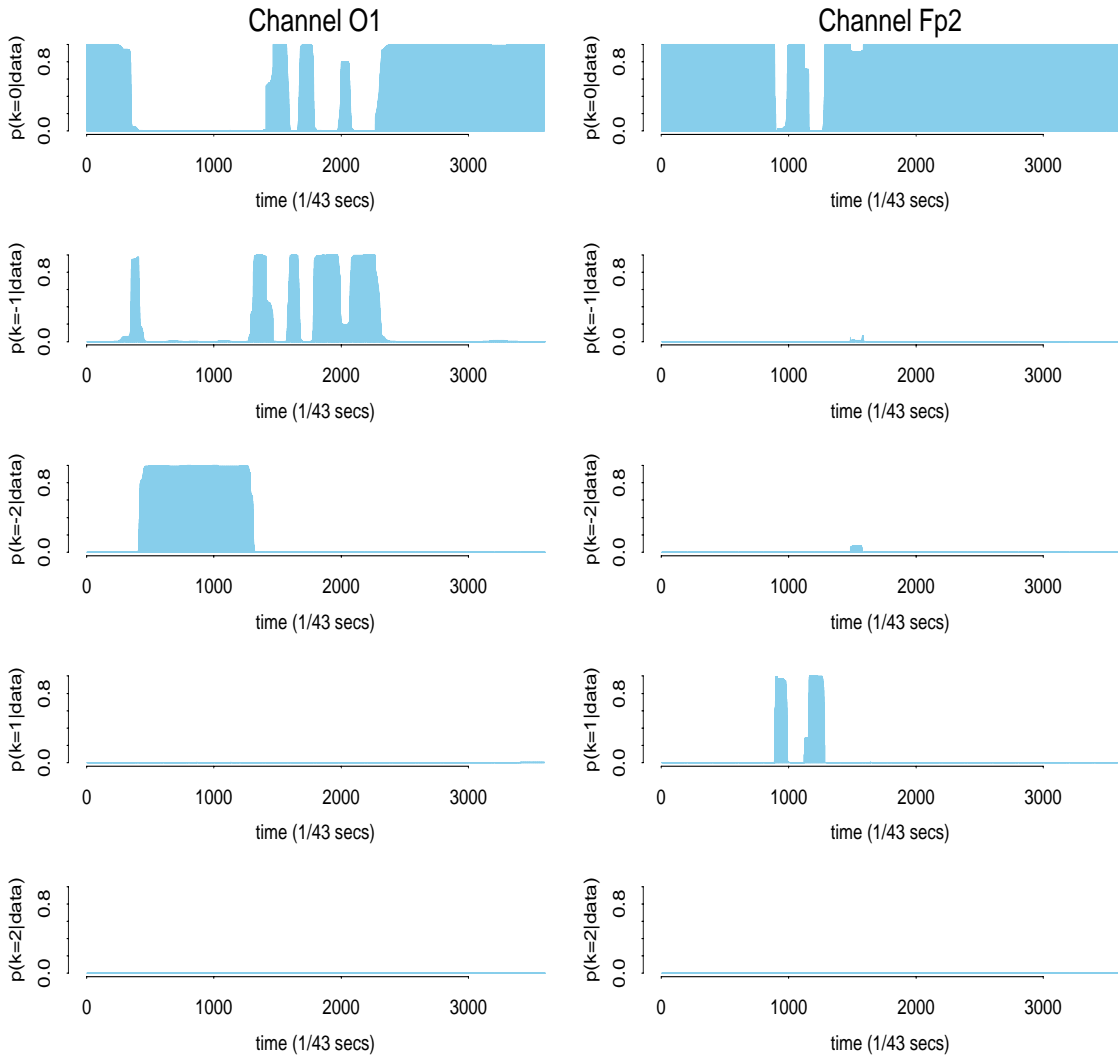


Figure 6: Estimated posterior probabilities of the lags/leads for channels O_1 and Fp_2 .

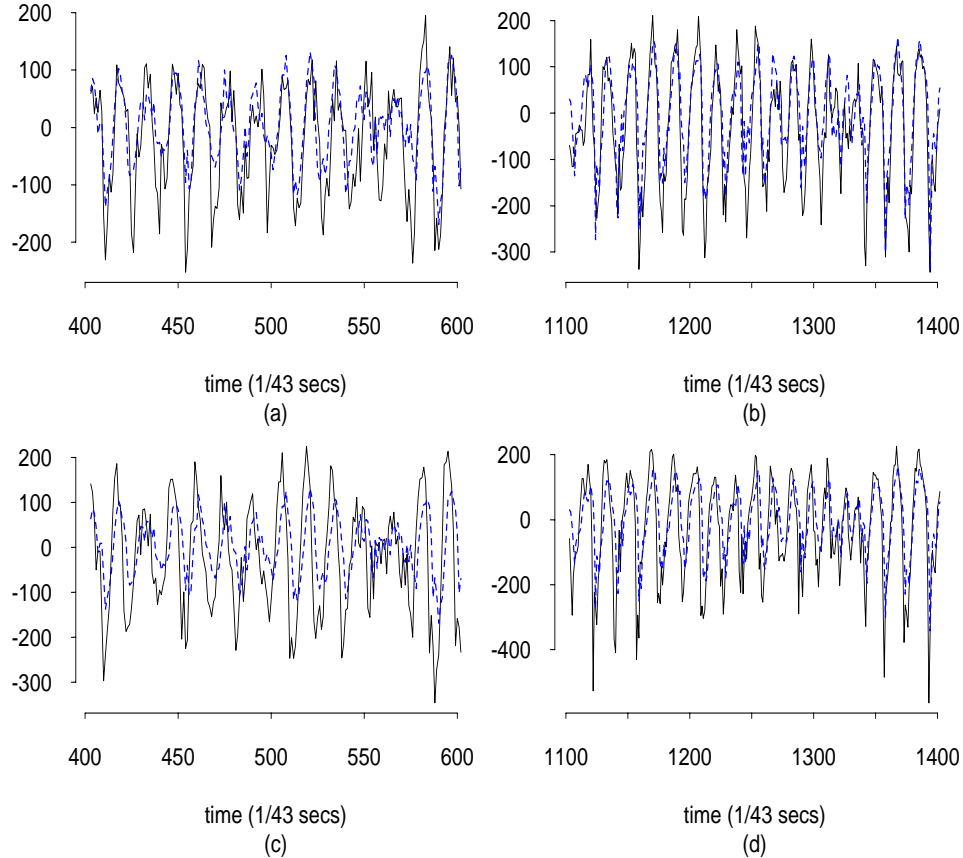


Figure 7: Estimated EEG traces obtained from the dynamic regression model for channel \mathbf{O}_1 (dotted lines) at different intervals during the seizure course. Frames (a) and (b) show the EEG trace recorded at site \mathbf{O}_1 (solid lines) and estimated trace obtained from the dynamic regression model (dotted lines) at early-middle (frame (a)) and middle (frame (b)) seizure periods. Frames (c) and (d) display the EEG trace recorded at the vertex (solid lines) and the estimated traces for channel \mathbf{O}_1 (dotted lines) for the same seizure periods displayed in frames (a) and (b).

residual autocorrelations tend to be more appreciable towards the end of the series. Uncertainty increases towards the dissipation of the seizure and these channels are “remote” with respect to the vertex. We believe this does not invalidate our modelling approach as the main interest here is in studying time intervals corresponding to major seizure activity. However, model refinements that capture this moderate “tail” correlation may be considered in the future, particularly if the focus is on studying the seizure dissipation period. For example, extensions of the models here that regress a given signal on various processes $x_{1,t}, \dots, x_{k,t}$ – for example, in addition to regressing any given channel on channel \mathbf{C}_z we may consider also other “neighbouring” channels – might be considered.

The posterior summaries presented confirm the existence of a spatio-temporal structure linking the EEG channels. Channels located closely exhibit similar features in terms of the recorded signals that vary over the seizure course. The transition probabilities and the

discount factors were chosen to impose smooth changes in the model parameters over time and even with such smoothness conditions it is possible to discover strong spatio-temporal patterns across the multiple signals.

4 Discussion

The analyses presented here demonstrate how these models may be used to explore the complex spatio-temporal structure underlying the Ictal19 EEG series. Previous univariate TVAR decompositions had suggested a common underlying structure characterised primarily by a persistent “seizure waveform” whose characteristic frequency lies consistently in the *delta* band, with values of 4 to 5Hz at the beginning of the seizure, decaying to much smaller values towards the end. Single factor models confirm this structure revealing also a spatial relation across the 19 EEG traces: signals recorded at channels located closer on the scalp have similar estimated factor weights. However, the need for models including more than two factors and possibly lagged values of such factors is highlighted by the structure of the residuals in the single factor models. Such developments are not easy, as the computational complexity and interpretability of factor models increases considerably with the number of factors.

Our alternative and quite novel dynamic regression models have proven useful in discovering the latent structure underlying the 19 EEG series. It is clear from the estimated lag/lead structure that an EEG signal recorded at a given site may exhibit time delays with respect to another signal recorded at a different scalp location and that these delays vary with time. Similarly, the values of the estimated regression coefficients are strongly related to the scalp location and the time interval considered. Models with more than one latent processes – for instance, models that explicitly introduce spatial dependence by regressing each channel on its “neighbouring” channels – and alternative structures for the class of transition probabilities models may be considered. Such developments are certainly of technical interest, though we are skeptical as to whether the additional modelling complexities will be at all worthwhile from the viewpoint of refining the interpretation and understanding of EEG traces.

In terms of EEG implications, our analysis suggests that dynamic regression models can usefully assist researchers in improving the analysis of multichannel EEG data in general, and the ECT seizure data in particular. Our models improves our ability to study inter-lead relationships dynamically over the course of an EEG recording compared with existing techniques. As an example, the application of dynamic regressions to a multichannel EEG ECT seizure recording allowed us to carry out the first continuous analysis of spatial inter-relationships among the channels over time, and to identify the regional expression of seizure activity, the degree of spatial inter-relatedness of EEG activity, and the inter-lead lead/lag structure as they vary substantially over the course of the seizure. In agreement with Krystal *et al.*, (1999), we found periods of consistent lead/lag structure in some seizures suggestive of physiological travelling waves of electrical activity in the neurons of the cerebral cortex. Additionally we are now able to demonstrate how this structure varies with time. This information has important implications for the physiologic mechanisms of generalized tonic-clonic seizures in terms of their manner of initiation, development, and propagation.

Further directions for research within the multivariate modelling framework are under consideration. The TVAR decomposition results described in Section 2 have a direct extension to the multivariate case (Prado 1998). Fitting fully Bayesian time-varying vector

autoregressions (TV-VAR) to the 19 EEG series and exploring the corresponding decompositions into latent processes would be of primary interest. This is connected with the work of W. Gersch and coauthors (e.g., Gersch 1987; Kitagawa and Gersch 1996) although these authors have focused on studying feedback and lags in multi-channel EEG data via exploration of the spectral densities implied by the time-varying models rather than on time domain features. Such developments and connections are currently under study.

A Appendix

A.1 Posterior sampling algorithms for factor models

Consider a model with k factors, m series and the following structure for $t = 1, \dots, n$:

- the observation equations for $i = 1, \dots, m$,

$$y_{i,t} = \beta_{(i,1)}x_{1,t} + \dots + \beta_{(i,k)}x_{k,t} + \nu_{i,t}; \quad \nu_{i,t} \sim N(\cdot|0, v)$$

- the structural equations for the k factors, that is, for $j = 1, \dots, k$

$$x_{j,t} = \phi_{(j,t,1)}x_{j,t-1} + \dots + \phi_{(j,t,p_j)}x_{j,t-p_j} + \eta_{j,t}; \quad \eta_{j,t} \sim N(\cdot|0, s_j)$$

- the system equations for $j = 1, \dots, k$

$$\phi_{j,t} = \phi_{j,t-1} + \omega_{j,t}; \quad \omega_{j,t} \sim N(\cdot|0, \mathbf{U}_{j,t})$$

with $\phi_{j,t}$ the vector of p_j TVAR coefficients related to the factor $x_{t,j}$; $\mathbf{U}_{j,t}$ are $p_j \times p_j$ matrices controlling the evolution of $\phi_{j,t}$ and $\nu_{i,t}$, $\eta_{j,t}$ and $\omega_{l,t}$ are independent and mutually independent innovations. We assume that the variance-covariance matrices $\mathbf{U}_{j,t}$ are known or specified by single discount factors (West and Harrison 1997) and that $r_j = s_j/v$ are known quantities for $j = 1, \dots, k$. Let $\mathbf{Y} = \{\mathbf{y}'_1, \dots, \mathbf{y}'_n\}$ with $\mathbf{y}'_t = (y_{1,t}, \dots, y_{m,t})$ be the full set of observations; $\mathbf{X} = \{X_{1,n}, \dots, X_{k,n}\}$ the set of latent factor values with $X_{j,n} = \{x_{j,1}, \dots, x_{j,n}\}$; $\mathbf{U} = \{\mathbf{U}_1, \dots, \mathbf{U}_k\}$ with $\mathbf{U}_j = \{\mathbf{U}_{j,1}, \dots, \mathbf{U}_{j,n}\}$; $\mathbf{B} = \{\beta'_1, \dots, \beta'_k\}$, the full set of factor weights with $\beta_j = (\beta_{(1,j)}, \dots, \beta_{(m,j)})'$ and $\Phi = \{\phi_1, \dots, \phi_k\}$, with $\phi_j = \{\phi_{j,1}, \dots, \phi_{j,n}\}$. In addition let $p(v)$, $p(\beta_j)$, $p(\phi_{j,0})$ and $p(x_{j,0} | X_{j,0}^j)$ for $j = 1, \dots, k$ denote the priors for the observational variance, the factor weights, the autoregressive coefficients and the k latent processes at $t = 0$. The Gibbs sampling scheme to generate posterior samples iterates through the set of complete conditional posteriors given as follows.

- Sample \mathbf{X} from $p(\mathbf{X} | \mathbf{Y}, \mathbf{B}, \Phi, v, s_1, \dots, s_k)$. This reduces to sampling $X_{j,n}$ from the conditional distribution $p(X_{j,n} | \mathbf{Y}, \mathbf{B}, \phi_k, v, s_1, \dots, s_k, \mathbf{X}(-X_{j,n}))$ for each j with $\mathbf{X}(-X_{j,n})$ the full set of factor processes values except $X_{j,n}$. Now, for each j we can write

$$\begin{aligned} \mathbf{z}_{j,t} &= \mathbf{B}_j \mathbf{q}_{j,t} + \nu_{j,t} \\ \mathbf{q}_{j,t} &= \mathbf{G}_{j,t} \mathbf{q}_{j,t-1} + \eta_{j,t}, \end{aligned}$$

with $\mathbf{z}_{j,t} = \mathbf{y}_t - \mathbf{B}_1 \mathbf{q}_{1,t} - \dots - \mathbf{B}_{j-1} \mathbf{q}_{j-1,t} - \mathbf{B}_{j+1} \mathbf{q}_{j+1,t} - \dots - \mathbf{B}_k \mathbf{q}_{k,t}$; $\mathbf{q}_{j,t} = (x_{j,t}, \dots, x_{j,t-p_j+1})'$; $\eta_{k,t} = (\eta_{k,t}, 0, \dots, 0)'$; $\eta_{j,t} \sim N(\cdot|0, v\mathbf{I})$; \mathbf{B}_k and $\mathbf{G}_{j,t}$ are $m \times p_j$ and $p_j \times p_j$ matrices,

$$\mathbf{B}_j = \begin{pmatrix} \beta_{(j,1)} & 0 & \dots & 0 \\ \vdots & \vdots & & \vdots \\ \beta_{(j,m)} & 0 & \dots & 0 \end{pmatrix}, \quad \mathbf{G}_{j,t} = \begin{pmatrix} \phi_{(j,t,1)} & \dots & \phi_{(j,t,p_j-1)} & \phi_{(j,t,p_j)} \\ 1 & \dots & 0 & 0 \\ \vdots & \ddots & \vdots & \vdots \\ 0 & \dots & 1 & 0 \end{pmatrix}.$$

Then, assuming a prior structure $p(\mathbf{q}_{j,0} | \mathbf{m}_{j,0}, \mathbf{C}_{j,0}) = N_{p_j}(\cdot | \mathbf{m}_{j,0}, \mathbf{C}_{j,0})$ the previous equations specify a standard multivariate normal DLM (West and Harrison 1997) so it is possible to sample $X_{j,n}$ with the following steps:

- Compute the moments $\mathbf{m}_{j,t}$ and $\mathbf{C}_{j,t}$ of the distributions $(\mathbf{q}_{j,t} \mid \mathbf{q}_{j,0}, \mathbf{z}_{j,1}, \dots, \mathbf{z}_{j,t}) = N_{p_j}(\cdot \mid \mathbf{m}_{j,t}, \mathbf{C}_{j,t})$ for $t = 1, \dots, n$;
- Sample $\mathbf{q}_{j,n}$ from $p(\mathbf{q}_{j,n} \mid \mathbf{m}_{j,n}, \mathbf{C}_{j,n}) = N_{p_j}(\cdot \mid \mathbf{m}_{j,n}, \mathbf{C}_{j,n})$;
- Given $\mathbf{q}_{j,t+1}$ replace the first $p_j - 1$ elements of $\mathbf{q}_{j,t}$. Compute the moments $m_{j,t-p_j+1}^*$ and $C_{j,t-p_j+1}^*$ of the marginal distribution of the last element of $\mathbf{q}_{j,t}$ from the full distribution $N_{p_j}(\cdot \mid \mathbf{m}_{j,t}, \mathbf{C}_{j,t})$ and sample the last element $x_{j,t-p_j+1}$ from the univariate normal distribution $N(x_{j,t-p_j+1} \mid \tilde{m}_{j,t-p_j+1}, \tilde{C}_{j,t-p_j+1})$ with

$$\begin{aligned}\tilde{m}_{j,t-p_j+1} &= m_{j,t-p_j+1}^* + \frac{C_{j,t-p_j+1}^* \phi_{(j,t+1,p_j)}}{\phi_{(j,t+1,p_j)}^2 C_{j,t-p_j+1}^* + s_j} \times \\ &\quad \times (x_{j,t+1}^* - \phi_{(j,t+1,p_j)} m_{j,t-p_j+1}^*) \\ \tilde{C}_{j,t-p_j+1} &= C_{j,t-p_j+1}^* - \frac{(C_{j,t-p_j+1}^* \phi_{(j,t+1,p_j)})^2}{\phi_{(j,t+1,p_j)}^2 C_{j,t-p_j+1}^* + s_j},\end{aligned}$$

where $x_{j,t+1}^* = x_{j,t+1} - \sum_{h=1}^{p_j-1} \phi_{(j,t+1,h)} x_{j,t+1-h}$ based on the value of $\mathbf{q}_{j,t+1}$ previously sampled. Repeat this step for $t = n - 1, \dots, 0$.

- Sample ϕ_j from $p(\phi_j \mid X_{j,n}, s_j, \mathbf{U}_j)$ for $j = 1, \dots, k$. For each j we have a DLM structure given by the equations

$$\begin{aligned}x_{j,t} &= \mathbf{F}'_{j,t} \phi_{j,t} + \eta_{j,t} \\ \phi_{j,t} &= \phi_{j,t-1} + \omega_{j,t},\end{aligned}$$

with $\mathbf{F}_{j,t} = (x_{j,t-1}, \dots, x_{j,t-p_j+1})'$. Efficient generation can be performed via forward-filter-backward-sampling algorithms (Carter and Kohn 1994; Frühwirth-Schnatter 1994)

- Sample v from $p(v \mid \mathbf{Y}, \mathbf{B}, \mathbf{X})$. For $i = 1, \dots, m$ and $j = 1, \dots, k$ compute

$$\begin{aligned}e_{i,y} &= \sum_{t=1}^n (y_{i,t} - \beta_{(i,1)} x_{1,t} - \dots - \beta_{(i,k)} x_{k,t}), \\ e_{j,x} &= \sum_{t=1}^n \sqrt{1/r_j} * (x_{j,t} - \phi_{(i,t,j)} x_{j,t-1} - \dots - \phi_{(j,t,p_j)} x_{j,t-p_j})\end{aligned}$$

and sample the posterior proportional to $p(v) v^{-(\alpha+1)} \exp\{-\beta/v\}$ with $\alpha = ((n * (m + k)/2) - 1)$ and $\beta = (\sum_{i=1}^m e_{i,y}^2)/2 + (\sum_{j=1}^k e_{j,x}^2/2r_j)$

- Sample \mathbf{B} from $p(\mathbf{B} \mid \mathbf{Y}, \mathbf{X}, v)$. Assuming a prior structure such that $p(\beta_1, \dots, \beta_k) = p(\beta_1) \dots p(\beta_k)$ this simplifies to sampling β_j for $j = 1, \dots, k$ from $p(\beta_j \mid \mathbf{Y}, \mathbf{X}, v, \mathbf{B}(-\beta_j))$. Then, for each j sample the posterior proportional to $p(\beta_j) \times \exp(-\sum_{t=1}^n \mathbf{u}'_{j,t} \mathbf{u}_{j,t}/2v)$ with $\mathbf{u}_{j,t} = \mathbf{y}_t - \beta_1 x_{1,t} - \dots - \beta_{j-1} x_{j-1,t} - \beta_{j+1} x_{j+1,t} - \dots - \beta_k x_{k,t}$. The restrictions on the factor weights should be considered when sampling from the posteriors.

A.2 Posterior sampling algorithms for dynamic regression models with time-varying lag/lead structures

In the model of equation (3), define $\mathbf{y}_i = \{y_{i,1}, \dots, y_{i,n}\}$, $\mathbf{x} = \{x_1, \dots, x_n\}$, $\beta_i = \{\beta_{(i,1)}, \dots, \beta_{(i,n)}\}$, $\mathbf{l}_i = \{l_{i,1}, \dots, l_{i,n}\}$ and $\mathbf{u}_i = \{u_{i,1}, \dots, u_{i,n}\}$. Let $p(l_{i,0})$, $p(\beta_{i,0})$ and $p(v_i)$ denote respectively the priors for the lag/lead at $t = 0$, the prior for the regression coefficients at $t = 0$ and the prior for the observational variance. The Gibbs sampling scheme to generate posterior samples iterates through the set of complete conditional posteriors given as follows.

- Sample β_i from $p(\beta_i | \mathbf{y}_i, \mathbf{x}, \mathbf{l}_i, v_i)$: conditional on $\mathbf{y}_i, \mathbf{x}, \mathbf{l}_i, v_i$ we have a DLM structure whose system parameter is the vector of regression coefficients β_i , therefore efficient generation can be obtained via forward-filter-backward-sampling.
- Sample \mathbf{l}_i from $p(\mathbf{l}_i | \mathbf{y}_i, \mathbf{x}, \beta_i, v_i)$: following Carter and Kohn (1994), in order to sample \mathbf{l}_i we sample $l_{i,n}$ from $p(l_{i,n} | \mathbf{y}_i, \mathbf{x}, \beta_i, v_i)$ and then for $t = n - 1, \dots, 1$ we sample from $p(l_{i,t} | l_{i,t+1}, \mathbf{y}_i^t, \mathbf{x}^t, \beta_i^t, v_i)$. A discrete filter is used to compute $p(l_{i,n} | \mathbf{y}_i, \mathbf{x}, \beta_i, v_i)$ and $p(l_{i,t} | l_{i,t+1}, \mathbf{y}_i^t, \mathbf{x}^t, \beta_i^t, v_i)$.
- Sample v_i from $p(v_i | \mathbf{y}_i, \mathbf{x}, \beta_i, \mathbf{l}_i)$: sample the conditional posterior distribution proportional to $p(v_i)v_i^{-(\alpha+1)} \exp(-\beta/v_i)$ with $\alpha = n/2 - 1$ and $\beta = (\sum_{t=1}^n e_{i,t}^2)/2$.

Bibliography

- Angeleri, F., Butler, S., Giaquinto, S. and Majkowski, J. (1997) *Analysis of the electrical activity of the brain*. Chischester; New York: Wiley.
- Brooks, S. P. and Roberts, G.O. (1999) Assessing convergence of Markov chain Monte Carlo algorithms. *Statistics and Computing*, **8**, 319–335.
- Carter, C.K. and Kohn, R. (1994) Gibbs sampling for state space models. *Biometrika*, **81**, 541–53.
- Dyro, F.M. (1989) *The EEG handbook*. Boston: Little, Brown and Co.
- Frühwirth-Schnatter, S. (1994) Data augmentation and dynamic linear models. *Journal of Time Series Analysis*, **15**, 183–102.
- Gersch, W. (1985) Modeling nonstationary time series and inferring instantaneous dependency, feedback and causality: An application to human epileptic seizure event data. In *Identification and System Parameter Estimation 1985, 7th IFAC/IFORS Symposium*, pp. 737–42. York, UK.
- Gersch, W. (1987) Non-Stationary multichannel time series analysis. In *EEG Handbook, Revised Series* (ed. A. Gevins), vol. 1, pp. 261–96. New York: Academic Press.
- Huerta, G. and West, M. (1999) Priors and component structures in autoregressive time series models. *Journal of the Royal Statistical Society-Series B*, **61**, 881–899.
- Kitagawa, G. and Gersch, W. (1996) *Smoothness Priors Analysis of Time Series*, Lecture Notes in Statistics, vol. 116. New York: Springer-Verlag.
- Krystal, A.D., Greenside, H.S., Weiner, R.D. and Gassert, D. (1996) A comparison of EEG signal dynamics in walking, after anesthesia induction and during electroconvulsive therapy seizures. *Electroenceph. Clin. Neurophysiol.*, **99**, 129–140.
- Krystal, A.D., Prado, R. and West, M. (1999) New methods of time series analysis of non-stationary eeg data: Eigenstructure decomposition of time varying autoregressions. *Clinical Neurophysiology*, **110**, 1–10.
- Krystal, A.D., West, M., Prado, R., Greenside, H.S., Zoldi, S. and Weiner, R.D. (1999) The EEG effects of ECT: Implications for rTMS. In *Progress in Neuropsychopharmacology and Biological Psychiatry* (to appear).
- Niedermeyer, E. (1993) Epileptic Seizure Disorders. In *Electroencephalography (3rd Edition)*, eds: E. Niedermeyer and F. Lopes da Silva, pp. 461–564. Baltimore: Williams and Wilkins.
- Peña, D. and Box, G.E.P (1987) Identifying a simplifying structure in time series. *Journal of the American Statistical Association*, **82**, 836–843.
- Prado, R. (1998) Latent structure in non-stationary time series. Ph.D. Thesis. Duke University, Durham, NC.

- Prado, R. and West, M. (1997) Exploratory modelling of multiple non-stationary time series: Latent process structure and decompositions. In *Modelling Longitudinal and Spatially Correlated Data*, ed: T.Gregoire. New York: Springer-Verlag.
- Staton, R.D., Prudic, J., Devanand, D.P. and Prudic, J. (1981) Stimulus intensity, seizure threshold and seizure duration: Impact on the efficacy and cognitive effects of electroconvulsive therapy. *New. Eng. J. Med.*, **328**, 803–843.
- Tiao, G. C. and Tsay, R.S. (1989) Model specification in multivariate time series with applications (with discussion). *Journal of the Royal Statistical Society*, **51**, 157–213.
- Troughton, P.T. and Godsill, S.J. (1997) Bayesian model selection for time series using Markov Chain Monte Carlo. Technical Report. Signal Processing and Communications Laboratory. Department of Engineering, University of Cambridge.
- Weiner, R. D., Coffey, E. and Krystal, A. D. (1991) The monitoring and management of electrically induced seizures. *Psychiatr. Clin. of North Am.*, **14**, 845–69.
- Weiner, R. D. and Krystal, A. D. (1993) EEG monitoring of ECT seizures. In *The Clinical Science of Electroconvulsive Therapy* (ed. C.E. Coffey), pp. 93–109. Washington, D.C.: American Psychiatric Press.
- Weiner, R. D. and Krystal, A. D. (1994) The present use of electroconvulsive therapy. *Ann. Rev. of Medicine*, **45**, 273–281.
- West, M. and Harrison, J. (1997) *Bayesian Forecasting and Dynamic Models*, 2nd edn. New York: Springer-Verlag.
- West, M., Prado, R. and Krystal, A.D. (1999) Evaluation and comparison of EEG traces: Latent structure in nonstationary time series. *J. Amer. Statist. Assoc.*, **94**, 375–387.
- Zoldi, S., Greenside, H.S. and Krystal, A.D. (1996) Redundancy and stationarity of 21-channel EEG data recorded during ECT seizures. *J. Clin. Neurophysiol.*, **5**, 440.